

Thermal Dark Photon Dark Matter, Coseattering, and Long-lived ALPs

Bastián Díaz Sáez^{a,b}

^a*Instituto de Física, Pontificia Universidad Católica de Chile, Avenida Vicuña Mackenna 4860, Santiago, Chile.*

^b*Millennium Institute for Subatomic Physics at the High-Energy Frontier (SAPHIR), Fernández Concha 700, Santiago, Chile.*

E-mail: bastian.diaz@uc.cl

ABSTRACT: We study thermal freeze-out in the *dark axion portal* - an axion coupling to the dark photon and photon - considering the dark photon as the lightest stable particle, thereby a dark matter candidate. We pay special attention to the coseattering regime, founding viable DM scenarios fulfilling the correct relic abundance. Furthermore, we explore the prospects of having the axion as a long-lived particle, possibly to be observed at the LHC and future detectors.

Contents

1	Introduction	1
2	Model	2
3	Relic abundance	2
3.1	Boltzmann equations	2
3.2	Relic abundance	3
4	Prospects for LLP	6
5	Conclusions	7

1 Introduction

Beyond Standard Model (BSM) scenarios predict the existence of new bosons of spin 0 and 1. In particular, the interplay of dark photons (DP) and axion-like particles (ALP) in the so-called *dark axion portal*, this is, when the ALP couples to a DP and a SM photon, has been the subject of several studies, ranging from astrophysical probes to dark matter [1–9].

In this work, we study the dark axion portal in a thermal regime: both particles are assumed to be in thermal equilibrium at high temperatures with the SM plasma, until they freeze-out due to the domination of the expansion of the universe. In particular, we focus on the cospattering [10], or also known as conversion-driven freeze-out [11] (for other scenarios based on cospattering see [12–17]). Cospattering relies on the fact that DM particle decouples via inelastic conversions with its heavier dark state via the fast collision with relativistic SM particles in the thermal bath. Once these type of interactions drops below the Hubble expansion rate, the chemical equilibrium (CE) within the dark sector is no longer support, and the DM freezes-out.

In this work, we focus on the case where the DP is the DM candidate, and the ALP behaves as a heavier mediator. We make use of `micrOMEGAs` code [18] to calculate the relic abundance of the DP. In some regions of the parameter space, especially when cospattering is the dominant thermal regime, the ALP lifetime significantly increases to the point to be considered as a *long-lived* particle (LLP). This makes cospattering a mechanism to be phenomenological testable at colliders [19, 20].

The paper is structured in the following way. In Sec. 2, we present the model. In Sec. 3, we study in detail the relic abundance of this scenario. In Sec. 4, we present the relevant constraints, along with the prospects of the axion as a LLP. Finally, in Sec. 5 we conclude our work.

2 Model

We extend the gauge sector of the SM with a $U(1)'$ gauge symmetry. As a result, there is a new gauge field A'_μ , and also we introduce a real pseudoscalar ϕ . We set that this scenario has a charge conjugation symmetry (also called dark CP symmetry) acting on the new fields as $\phi \rightarrow -\phi$ and $A'_\mu \rightarrow -A'_\mu$, and the SM fields transforming trivially under it [5] (also see [21, 22]). In this way, the Lagrangian of this SM extension is given by:

$$\mathcal{L} \supset -\frac{1}{4}F_{\mu\nu}F^{\mu\nu} - \frac{1}{4}F'_{\mu\nu}F'^{\mu\nu} - \frac{1}{2}m_{\gamma'}^2 A'^2_\mu + \frac{1}{2}(\partial_\mu\phi)^2 - \frac{1}{2}m_\phi^2\phi^2 - \lambda_\phi\phi^4 - \lambda_{HS}\phi^2|H|^2, \quad (2.1)$$

with $(m_\phi, \lambda_\phi) > 0$, $F_{\mu\nu}$ the $U(1)_{em}$ photon field strength, and H the Higgs doublet of the SM. Due to the symmetry of this scenario, there is no kinetic mixing between A_μ and A'_μ , and it is allowed the following five-dimensional operator:

$$\mathcal{L}_5 = \frac{g_D}{4}\phi F'_{\mu\nu}\tilde{F}^{\mu\nu}, \quad (2.2)$$

where g_D is a dimensionfull parameter, sometimes related to a high energy scale as $f_D = 1/g_D$, and $\tilde{F}^{\mu\nu}$ being the dual field strength defined as $\tilde{F}^{\mu\nu} = \frac{1}{2}\epsilon^{\mu\nu\alpha\beta}F_{\alpha\beta}$. We remain agnostic about the possible UV origin of the five-dimensional operator. The new singlet scalar ϕ behaves as a unstable state which does not acquire any vacuum expectation value. Besides, we set $m_{\gamma'} < m_\phi$, such that the DP is cosmologically stable, and therefore the DM candidate. The inverse scenario is perfectly possible, rendering ϕ as the DM candidate, but we do not explore such possibility in this paper. In the following, we consider as independent parameters $(m_{\gamma'}, m_\phi, g_D, \lambda_{HS})$, and we make use of the useful parameter $\Delta m \equiv m_\phi - m_{\gamma'}$.

3 Relic abundance

In this section we solve the general set of cBE of γ' and ϕ making use of `micrOMEGAs` 6.0.4, which assumes that both particles were in CE at high temperatures. We implement this scenario assuming three thermal systems: the SM, the DM candidate γ' , and ϕ the heavier state.

3.1 Boltzmann equations

Introducing the independent variable $x = m_{\gamma'}/T$, the coupled Boltzmann equations (cBE) for the yields of γ' and ϕ , $Y_{\gamma'}$ and Y_ϕ , respectively, are given by

$$\frac{dY_{\gamma'}}{dx} = \frac{1}{3H} \frac{ds}{dx} \left[\langle\sigma_{\gamma'\gamma'00}v\rangle (Y_{\gamma'}^2 - Y_{\gamma',e}^2) + \langle\sigma_{\gamma'\phi00}v\rangle (Y_{\gamma'}Y_\phi - Y_{\gamma',e}Y_{\phi,e}) + \frac{\Gamma_{\gamma'\rightarrow\phi}}{s} \left(Y_{\gamma'} - Y_\phi \frac{Y_{\gamma',e}}{Y_{\phi,e}} \right) + \frac{\Gamma_\phi}{s} \left(Y_\phi - Y_{\gamma'} \frac{Y_{\phi,e}}{Y_{\gamma',e}} \right) \right], \quad (3.1)$$

$$\frac{dY_\phi}{dx} = \frac{1}{3H} \frac{ds}{dx} \left[\langle\sigma_{\phi\phi00}v\rangle (Y_\phi^2 - Y_{\phi,e}^2) + \langle\sigma_{\gamma'\phi00}v\rangle (Y_{\gamma'}Y_\phi - Y_{\gamma',e}Y_{\phi,e}) - \frac{\Gamma_{\gamma'\rightarrow\phi}}{s} \left(Y_{\gamma'} - Y_\phi \frac{Y_{\gamma',e}}{Y_{\phi,e}} \right) - \frac{\Gamma_\phi}{s} \left(Y_\phi - Y_{\gamma'} \frac{Y_{\phi,e}}{Y_{\gamma',e}} \right) \right], \quad (3.2)$$

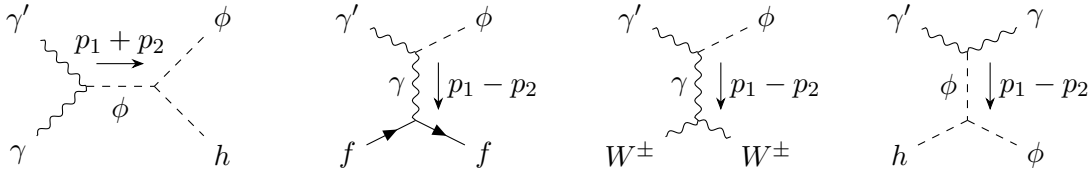


Figure 1: Tree-level contributions to $\gamma' \rightarrow \phi$ conversions.

where 0 denotes SM particles, and the equilibrium yields are

$$Y_{\gamma',e}(x) = \frac{45}{4\pi^4} \frac{x^2}{g_{*S}(x)} K_2(x), \quad (3.3)$$

$$Y_{\phi,e}(x) = \frac{45}{4\pi^4} \frac{1}{g_{*S}(x)} \left(\frac{m_\phi x}{m'_{\gamma'}} \right)^2 K_2 \left(\frac{m_\phi x}{m'_{\gamma'}} \right), \quad (3.4)$$

with $K_1(x)$ and $K_2(x)$ the Bessel second order functions, $g_{*S}(x)$ the effective number degrees in entropy, $s = \frac{2\pi^2}{45} g_{*S} T^3$ the entropy density in the universe, and H the Hubble rate in a radiation dominated universe. The rate of particle conversions per DM particle is given by

$$\Gamma_{\gamma' \rightarrow \phi} = \sum_{k,l} \langle \sigma_{\gamma' k \rightarrow \phi l v} \rangle n_{k,e}, \quad (3.5)$$

with k and l being a SM state (see the diagrams in Fig. 1), and Γ_ϕ is the thermally averaged decay rate of ϕ . As the SM photon is massless, all the ϕ decays in this scenario are on-shell. In order to quantify the relevance of `darkOmegaN` calculation, we make use of the function defined as $\Delta_{1s} \equiv 1 - \frac{\Omega h^2(1 \text{ sector})}{\Omega h^2(2 \text{ sectors})}$ [23], with $\Omega h^2(1 \text{ sector})$ obtained using the `darkOmega` function of `micrOMEGAS`, and $\Omega h^2(2 \text{ sectors})$ with `darkOmegaN`. Finally, in some parts of the paper we refer to the correct relic abundance as the one measured by Planck collaboration $\Omega_c h^2 = 0.12$ [24], which theoretically is obtain by

$$\Omega h^2 = \frac{2.9713 \times 10^9}{10.5115 \text{ GeV}} m_{\gamma'} Y_{\gamma',\infty}, \quad (3.6)$$

with $Y_{\gamma',\infty}$ the yield obtained after the freeze-out (FO) of the DM.

3.2 Relic abundance

For $T \lesssim (m_{\gamma'}, m_\phi)$, if the coupling g_D is sufficiently small, the CE between γ' and ϕ is broken, such that one must solve the cBE shown in eq. 3.1. In that regime, the heavier state ϕ remains in CE with the SM longer, since it presents additional interactions via the Higgs portal. For simplicity, we fix $\lambda_{HS} = 1$, although later we relax this assumption. In this way, the relic abundance depends only on three parameters, $(m_{\gamma'}, m_\phi, g_D)$. As we focus on the EW mass scale for the new states, we scan the relic abundance for $m_{\gamma'} = 100, 500$ and 1000 GeV over g_D . The results obtained with `darkOmegaN` (red curves) are shown in Fig. 2, for different values of Δm . In each case, three regimes are clearly noticed, typically known as cospattering (region I), mediator freeze-out (region II), and DM (co)annihilations (region III). In the cospattering regime, the relic abundance in each case depends strongly

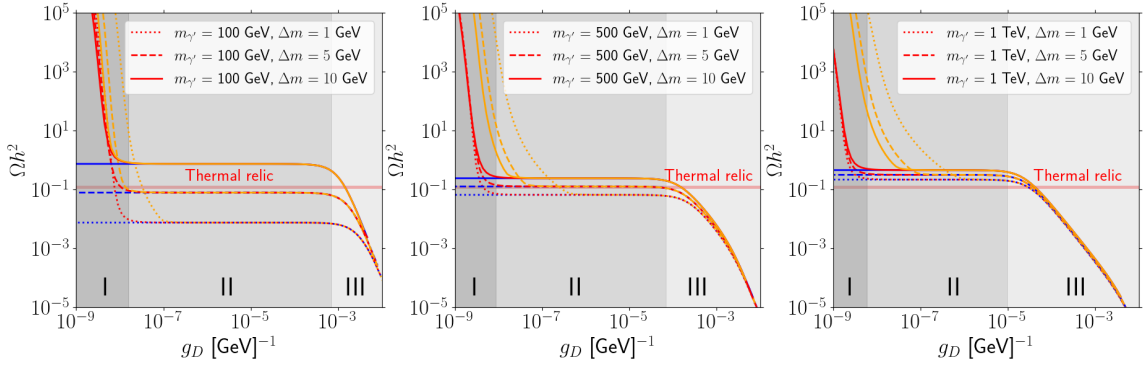


Figure 2: Relic abundance as a function of g_D for different masses of the dark photon and the mass shift. The red curves are obtained with `darkOmegaN`, the blue ones with `darkOmega`, and the orange ones without considering the process 1020 in eqs. 3.1. The regions shown in each plot as I, II and III, correspond to the case of $\Delta = 5 \text{ GeV}$. In all the plots we have set $\lambda_{HS} = 1$.

on g_D and too slightly on the mass difference, independent on the mass of the DM. For comparison, in each case we show the results obtained with `darkOmega` (blue lines), where the underlying assumption of this solver is CE for all the values of g_D . In this way, CE is always present in regions II and III. One more important thing to highlight here is the following. As in region II we have mediator FO, this is, the ALP which triggering the relic abundance via $\langle \sigma_{eff} v \rangle \propto e^{-2x_f \Delta m / m_{\gamma'}} \langle \sigma_{\phi\phi 00} v \rangle$, it indicates that the bigger is the mass system, the smaller is the spread of the relic abundances for a fixed Δm , an effect clearly visible when comparing each plot of Fig. 2. On the other hand, $\Delta m \lesssim 10 \text{ GeV}$, otherwise an overabundance is obtained.

With respect to the importance of decays in the CE between the DP and the ALP, we have also added the results obtained with `darkOmegaN`, but this time taking away cospattering conversion processes via `Excluding2010`, this is, excluding processes of the form $\gamma' 0 \leftrightarrow \phi 0$. The results are shown by the orange lines in each plot of Fig. 2. As a result, to maintain CE within the dark sector, decays requires normally higher g_D values than conversion processes $2 \rightarrow 2$, and the effectiveness of the decays to maintain CE increases with Δm , due to the increment of the decay phase space.

As in this work we pay more attention to the cospattering regime, in Fig. 3 (left) we show the yield evolution for a point in region I of Fig. 2 (left): $(m_{\gamma'}, m_\phi) = (100, 105) \text{ GeV}$ and $g_D = 10^{-8} \text{ GeV}^{-1}$. Notice the early yield departure of the DP from the equilibrium $Y_{\gamma',e}$, typical of the cospattering regime, whereas the departures of Y_ϕ from its equilibrium occurs at later x , since ϕ is in CE with the Higgs sector. In Fig. 3 (right), we show the quotient between the interaction rates for the relevant processes over the Hubble expansion rate. As it can be noted, conversions (orange line) remains below the Hubble rate for all x range.

Furthermore, to obtain a much more broad picture of the relic abundance behavior as a function of the parameters, in Fig. 4 we show the dependence of the relic abundance on

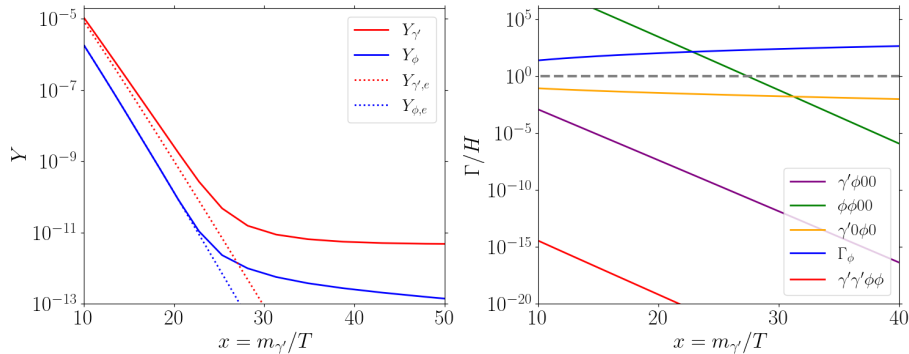


Figure 3: (left) Yield evolution for the DP and the ALP as a function of the inverse of the temperature. Here we consider $m_{\gamma'} = 100$ GeV, $\Delta m = 5$ GeV, $g_D = 10^{-8}$ GeV $^{-1}$ and $\lambda_{HS} = 1$. (right) Particle interactions rates over Hubble rate as a function of the inverse temperature. "0" here refers to a SM particle.

the DP mass (top row) and on λ_{HS} (bottom row), with the plot columns having different values of g_D . Notice that the chosen values for g_D in each column were based on the typical values found in the first scan (see Fig. 2) in the corresponding regions I, II and III, respectively. In the top left plot, as $g_D = 6 \times 10^{-9}$ GeV $^{-1}$, there are sharp differences obtained with `darkOmegaN` (red lines) and `darkOmega` (blue lines), where the former gives the correct result, since CE is lost in this regime. For middle and right plots of the first row, the match between the red and blue curve is practically in the whole range of masses, due to the fact that CE is recovered for such values of g_D . The inverted peak at $m_h/2$ in the second and third plot becomes sharper as Δm decreases, since in that regime coannihilations are stronger, and therefore the annihilation $\phi\phi$ via an on-shell Higgs becomes efficient. For higher values of DP masses, $m_{\gamma'} \gtrsim 100$ GeV, the overall resulting effect of increasing g_D varies depending on the thermal regime. For instance, as (co)annihilations are not effective in the mediator FO regime (middle plot), increasing $m_{\gamma'}$ makes that the relic abundance tend to increment independent on Δm , contrary to the decreasing behavior of the relic in the plot in the right, where coannihilations become more effective.

On the other hand, in Fig. 4 (bottom), we observe deviations in the relic abundance as a function of λ_{HS} , where we have fixed $m_{\gamma'} = 500$ GeV. Constant relic abundance is simply due to the fact that there are other processes participating in the freeze-out which do not depend on λ_{HS} , therefore dominating the relic abundance calculation for small enough values of this parameter. From these three plots, we observe that only certain sizable values for λ_{HS} give the correct relic abundance, and in certain cases, as shown by the last plot, none value of λ_{HS} will give the correct relic abundance. We do not expect strong deviations of these conclusions if we change $m_{\gamma'}$ in the mass range in between $m_h/2$ and 1 TeV, with the exception of the Higgs resonance, where more sharp numerical deviations are present.

In summary, in this section we have established the cBE of the system DP-ALP, showing that the three thermal decoupling phases appear, depending mainly on g_D : coscattering, mediator FO, and (co)annihilations. Furthermore, we have explored in detail the relic

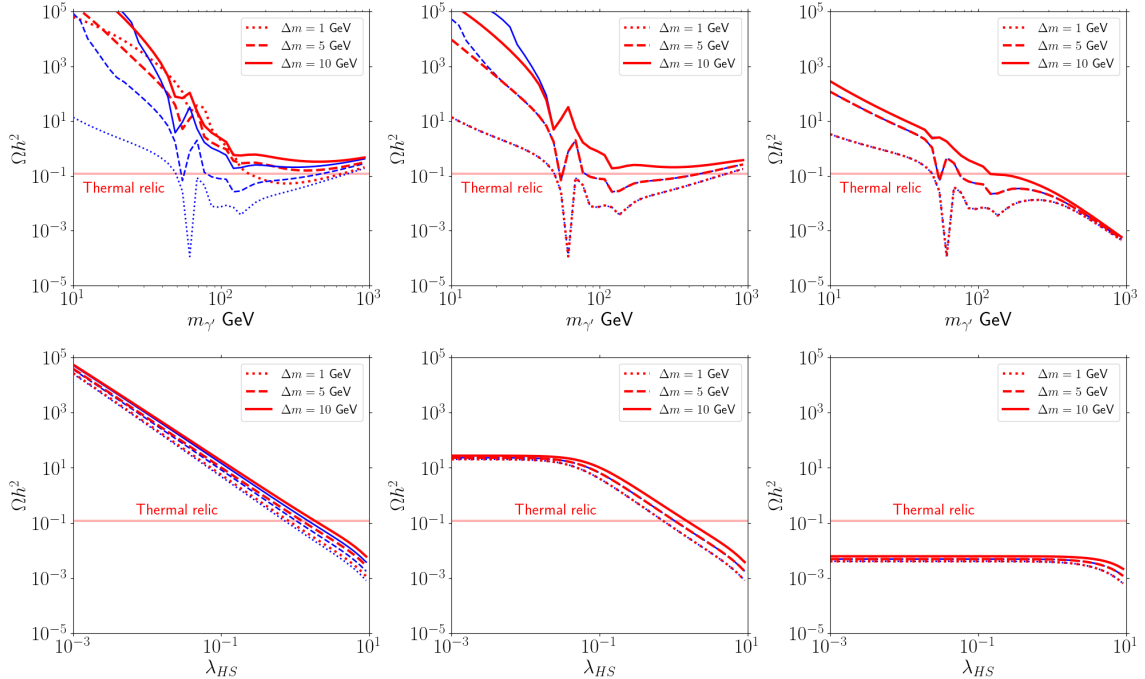


Figure 4: (top) Relic abundance as a function of $m_{\gamma'}$. In the left, middle and right columns we consider $g_D = 6 \times 10^{-9} \text{ GeV}^{-1}$, 10^{-5} GeV^{-1} and 10^{-3} GeV^{-1} , respectively. The red and blue lines are obtained with `darkOmegaN` and `darkOmega`, respectively. Here we set $\lambda_{HS} = 1$. (bottom) Relic abundance as a function of λ_{HS} , for $m_{\gamma'} = 500 \text{ GeV}$. The values of g_D follows the same order than the top row of plots.

abundance behavior as a function of the parameters of the model, founding parameter space that successfully achieve the correct relic abundance.

4 Prospects for LLP

As we have already seen in the previous section, having context the system DP-ALP in a thermal paradigm for masses above 10 GeV, one is able to obtain the correct relic abundance in vast regions of the parameter space. In particular, cospattering and mediator FO regimes present g_D and Δm small enough to establish the ALP ϕ as a long-lived particle (LLP). To explore the viability of having LLP with masses accessible to the LHC, we focus on electroweak scale masses for the new states, and values of g_D which give rise to cospattering and mediator FO regimes. In particular, we scan $m_{\gamma'} = [100, 500] \text{ GeV}$, $\Delta m = [0, 10] \text{ GeV}$, $g_D = [5 \times 10^{-9}, 3 \times 10^{-8}] \text{ GeV}^{-1}$, and $\lambda_{HS} = 1$, choosing the parameter space points which fulfill the correct relic abundance.

In Fig. 5 (left), we show these results, with each color point indicating the value of Δ_{1s}^Ω (the higher is this quantity, the most important cospattering is). Notice that, in general, the cospattering favors small mass shifts. Diagrams containing an on-shell Higgs in the initial or final state of processes $2 \rightarrow 2$ are not kinematically possible as long as $m_{\gamma'} \lesssim m_h$, then the abrupt change in the curves at that DP masses. On the other hand, in Fig. 5 (right) we

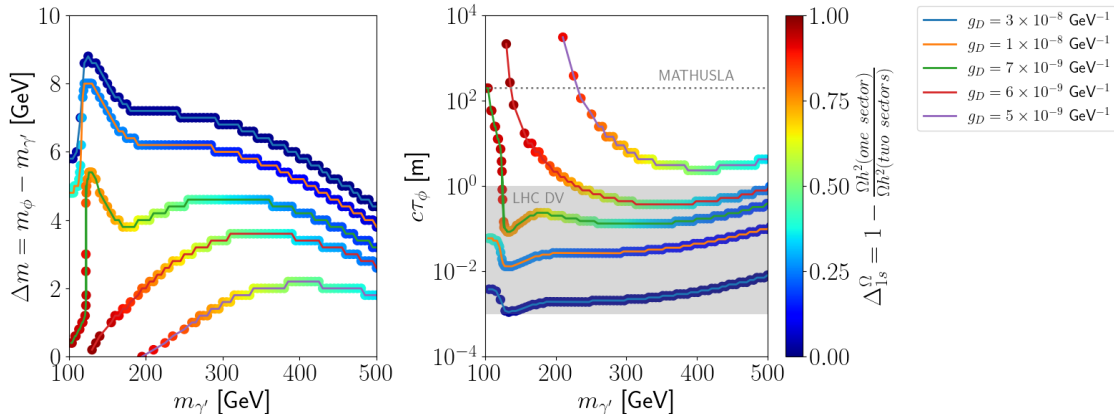


Figure 5: Points fulfilling the correct relic abundance measured by Planck [25]. The values of g_D were chosen such that all the points reach either the cospattering or mediator FO regimes. The color of each point represents Δ_{1s}^{Ω} . Here we have set $\lambda_{HS} = 1$. In the plot in the right, we highlight the expected distance of MATHUSLA [19] from the proton-proton colliding point, and the region expected for displace vertex (DV) in the detectors at the LHC.

project the points in the $(m_{\gamma'}, c\tau)$ plane, showing that in general, cospattering give rise to the longest lifetimes, with some points reaching distances of proposed future experiments such as MATHUSLA [19]. Notice that some of the predictions, e.g. $g_D = 7 \times 10^{-9} \text{ GeV}^{-1}$, give rise to ALPs with $c\tau$ in the reach of the LHC as displaced vertices (DV) [26]. Higher values of g_D are also in the reach of the LHC but in the mediator FO regime, as for instance the set of points on the orange and blue lines. At hadron colliders, one may pair produce ALPs via the chain $pp \rightarrow h^*(+X) \rightarrow \phi + \phi(+X)$ [27], with h^* an off-shell Higgs, and X associated states. In this case, the ALP, ϕ , may decay as a DV as $\phi \rightarrow \gamma' + \gamma$, with the signal $2\gamma + \cancel{E}$. A detailed analysis of the statistical significance of each signal contrasted with the corresponding backgrounds at the LHC is left for a future work.

5 Conclusions

In this work, we have investigated the thermal dark matter regime of a DP-ALP-photon system (aka dark axion portal), with the three particles interacting via a five-dimensional operator. We focused in the case where the DP plays the role of the DM candidate, whereas the ALP is a slightly heavier state which also interacts with the Higgs boson at tree-level. We have shown that, this scenario predicts the correct relic abundance for DP masses around of the electroweak scale up to the TeV scale. We have distinguished the three thermal regimes in the present model: cospattering, mediator FO, and DM (co)annihilations. As we have paid special attention to the two first regimes, the lifetime of the ALP increases enough to be considered as a LLP, presenting possible DV at the LHC detectors, and enough long-lived to reach detectors such as MATHUSLA. In the parameter space we focused on in this

work, it turns out that $g_D \ll 1 \text{ GeV}^{-1}$, thereby the leading one-loop cross section relevant for direct detection is highly suppressed, then not relevant for the analysis here¹.

Acknowledgments

B.D.S has been founded by ANID (ex CONICYT) Grant No. 3220566.

References

- [1] K. Kaneta, H.-S. Lee and S. Yun, *Portal Connecting Dark Photons and Axions*, *Phys. Rev. Lett.* **118** (2017) 101802 [[1611.01466](#)].
- [2] K. Kaneta, H.-S. Lee and S. Yun, *Dark photon relic dark matter production through the dark axion portal*, *Phys. Rev. D* **95** (2017) 115032 [[1704.07542](#)].
- [3] P. Deniverville, H.-S. Lee and Y.-M. Lee, *New searches at reactor experiments based on the dark axion portal*, *Phys. Rev. D* **103** (2021) 075006 [[2011.03276](#)].
- [4] P. Arias, A. Arza, J. Jaeckel and D. Vargas-Arancibia, *Hidden Photon Dark Matter Interacting via Axion-like Particles*, *JCAP* **05** (2021) 070 [[2007.12585](#)].
- [5] A. Hook, G. Marques-Tavares and C. Ristow, *Supernova constraints on an axion-photon-dark photon interaction*, *JHEP* **06** (2021) 167 [[2105.06476](#)].
- [6] J.C. Gutiérrez, B.J. Kavanagh, N. Castelló-Mor, F.J. Casas, J.M. Diego, E. Martínez-González et al., *Cosmology and direct detection of the Dark Axion Portal*, [2112.11387](#).
- [7] A. Hook, G. Marques-Tavares and C. Ristow, *CMB Spectral Distortions from an Axion-Dark Photon-Photon Interaction*, [2306.13135](#).
- [8] H. Hong, U. Min, M. Son and T. You, *A cosmic window on the dark axion portal*, *JHEP* **03** (2024) 155 [[2310.19544](#)].
- [9] K. Jodłowski, *Looking forward to photon-coupled long-lived particles II: dark axion portal*, [2305.10409](#).
- [10] R.T. D’Agnolo, D. Pappadopulo and J.T. Ruderman, *Fourth Exception in the Calculation of Relic Abundances*, *Phys. Rev. Lett.* **119** (2017) 061102 [[1705.08450](#)].
- [11] M. Garny, J. Heisig, B. Lülfi and S. Vogl, *Coannihilation without chemical equilibrium*, *Phys. Rev. D* **96** (2017) 103521 [[1705.09292](#)].
- [12] H.-C. Cheng, L. Li and R. Zheng, *Coscatting/Coannihilation Dark Matter in a Fraternal Twin Higgs Model*, *JHEP* **09** (2018) 098 [[1805.12139](#)].
- [13] F. Brümmer, *Coscatting in next-to-minimal dark matter and split supersymmetry*, *JHEP* **01** (2020) 113 [[1910.01549](#)].
- [14] S. Junius, L. Lopez-Honorez and A. Mariotti, *A feeble window on leptophilic dark matter*, *JHEP* **07** (2019) 136 [[1904.07513](#)].

¹In the opposite hierarchy, where the ALP is the lightest stable state $m_\phi < m_{\gamma'}$, then the DM candidate, ϕ could be subject to strong tree-level direct detection rates through the Higgs portal. This other hierarchy will be addressed in a future work.

- [15] J. Heeck, J. Heisig and A. Thapa, *Dark matter and radiative neutrino masses in conversion-driven scotogenesis*, *Phys. Rev. D* **107** (2023) 015028 [[2211.13013](#)].
- [16] J. Heisig, A. Lessa and L.M.D. Ramos, *Probing conversion-driven freeze-out at the LHC*, [2404.16086](#).
- [17] B. Díaz Sáez, J. Lahiri and K. Möhling, *Cosattering in the Extended Singlet-Scalar Higgs Portal*, [2404.19057](#).
- [18] G. Belanger, F. Boudjema, A. Pukhov and A. Semenov, *MicrOMEGAs: A Program for calculating the relic density in the MSSM*, *Comput. Phys. Commun.* **149** (2002) 103 [[hep-ph/0112278](#)].
- [19] D. Curtin et al., *Long-Lived Particles at the Energy Frontier: The MATHUSLA Physics Case*, *Rept. Prog. Phys.* **82** (2019) 116201 [[1806.07396](#)].
- [20] G. Cottin, *LLP overview: theory perspective*, *PoS LHCP2023* (2024) 164.
- [21] E. Ma, *Inception of Self-Interacting Dark Matter with Dark Charge Conjugation Symmetry*, *Phys. Lett. B* **772** (2017) 442 [[1704.04666](#)].
- [22] M. Duerr, K. Schmidt-Hoberg and S. Wild, *Self-interacting dark matter with a stable vector mediator*, *JCAP* **09** (2018) 033 [[1804.10385](#)].
- [23] G. Alguero, G. Belanger, S. Kraml and A. Pukhov, *Co-scattering in micrOMEGAs: a case study for the singlet-triplet dark matter model*, [2207.10536](#).
- [24] PLANCK collaboration, *Planck 2018 results. VI. Cosmological parameters*, *Astron. Astrophys.* **641** (2020) A6 [[1807.06209](#)].
- [25] Planck collaboration, N. Aghanim et al., *Planck 2018 results. VI. Cosmological parameters*, [1807.06209](#).
- [26] J. Alimena et al., *Searching for long-lived particles beyond the Standard Model at the Large Hadron Collider*, *J. Phys. G* **47** (2020) 090501 [[1903.04497](#)].
- [27] N. Craig, H.K. Lou, M. McCullough and A. Thalappilil, *The Higgs Portal Above Threshold*, *JHEP* **02** (2016) 127 [[1412.0258](#)].